Journal of Groundwater Science and Engineering
ISSN 2305-7068
Indexed by ESCI CABI CSA
Scopus GeoRef AJ CNKI

A signal decomposition optimized SWAT+ coupling framework for simulating groundwater response in the central plains agricultural core area: Sensitivity and land use scenarios

Jia-wen Liu, Xian-qi Zhang

Citation:
Liu JW, Zhang XQ. 2026. A signal decomposition optimized SWAT+ coupling framework for simulating groundwater response in the central plains agricultural core area: Sensitivity and land use scenarios. Journal of Groundwater Science and Engineering, 14(4): 518-534.

View online: https://doi.org/10.26599/JGSE.2026.9280092

Articles you may be interested in

Groundwater recharge modeling with integration of land use/land cover and climate change projections in Surakarta City, Indonesia
Journal of Groundwater Science and Engineering. 2025, 13(4): 352-370 https://doi.org/10.26599/JGSE.2025.9280059

Groundwater level response to different withdrawal scenarios (Case study: Talesh Aquifer, Iran)
Journal of Groundwater Science and Engineering. 2026, 14(2): 199-212 https://doi.org/10.26599/JGSE.2026.9280079

Modelling the monthly hydrological balance using Soil and Water Assessment Tool (SWAT) model: A case study of the Wadi Mina upstream watershed
Journal of Groundwater Science and Engineering. 2024, 12(2): 161-177 https://doi.org/10.26599/JGSE.2024.9280013

Determination of water balance equation components in irrigated agricultural watersheds using SWAT and MODFLOW models : A case study of Samalqan plain in Iran
Journal of Groundwater Science and Engineering. 2022, 10(1): 44-56 https://doi.org/10.19637/j.cnki.2305-7068.2022.01.005

Evaluation of shallow geothermal energy resources in the Beijing-Tianjin-Hebei Plain based on land use
Journal of Groundwater Science and Engineering. 2021, 9(2): 129-139 https://doi.org/10.19637/j.cnki.2305-7068.2021.02.005

Sensitivity assessment of strontium isotope as indicator of polluted groundwater for hydraulic fracturing flowback fluids produced in the Dameigou Shale of Qaidam Basin
Journal of Groundwater Science and Engineering. 2021, 9(2): 93-101 https://doi.org/10.19637/j.cnki.2305-7068.2021.02.001

Journal of Groundwater Science and Engineering 14(2026) 518–534

Journal homepage: http://gwse.iheg.org.cn

Research Article

A signal decomposition optimized SWAT+ coupling framework for simulating groundwater response in the central plains agricultural core area: Sensitivity and land use scenarios

Jia-wen Liu[1*], Xian-qi Zhang[1,2,3]

[1] *Water Conservancy College, North China University of Water Resources and Electric Power, Zhengzhou* 450046, *China*.
[2] *Collaborative Innovation Center of Water Resources Efficient Utilization and Protection Engineering, Zhengzhou* 450046, *China*.
[3] *Technology Research Center of Water Conservancy and Marine Traffic Engineering, Henan Province, Zhengzhou* 450046, *China*.

Abstract: Predicting groundwater depth is crucial for sustainable water management in agricultural regions facing intensive irrigation and rapid urbanization. Traditional data-driven models lack physical interpretability, while physical models like SWAT+ often struggle with non-stationary inputs, limiting their accuracy. This study proposes a novel Physics-Dominated Signal Decomposition Optimization (PD-SDO) framework that integrates SWAT+ with Extreme-point Symmetric Mode Decomposition (ESMD) to integrate physical mechanisms with data optimization. The framework is specifically designed for intensively managed mixed land-use regions, exemplified by the study area—a national strategic zone for agricultural development. Key innovations include: 1) ESMD-optimized inputs that extract high-frequency components (the first intrinsic mode function (Intrinsic Mode Function 1, IMF1), representing the highest-frequency component of the decomposed precipitation series) from precipitation to capture extreme rainfall pulses (>50 mm/d), thereby enhancing SWAT+'s adaptability to non-stationary climatic forcings prevalent in monsoon-influenced areas; 2) sensitivity-guided analysis identifying ALPHA_BF as the dominant parameter controlling groundwater recharge, which, combined with spatial heterogeneity analysis, reveals dual-mode drainage dynamics in loess-dominated unsaturated zones; 3) A closed-loop optimization where residual analysis dynamically adjusts ESMD thresholds, enabling model self-optimization; 4) Quantified land-use impacts showing contrasting hydrological effects under afforestation and urbanization scenarios, providing direct insights for spatial planning. The framework significantly improves simulation accuracy for groundwater depth, achieving a Nash-Sutcliffe Efficiency (NSE) of 0.94 and a Mean Absolute Error (MAE) of 8.02 m, which represents a 23% gain over the standalone SWAT+. It also enhances computational efficiency by 40% with minimal accuracy loss and provides 2.3× greater physical interpretability than pure black-box models. PD-SDO offers a replicable solution for high-fidelity groundwater modeling in rapidly changing mixed land-use zones, effectively balancing mechanistic fidelity with predictive performance. The framework and its findings provide a scientific basis for optimizing water allocation and land use management within strategic agricultural regions.

Keywords: Groundwater depth; SWAT+; Parameter sensitivity; Land use scenarios; Signal decomposition; Agricultural Core Area

Received: 23 Jul 2025/ Accepted: 08 Apr 2026/ Published: 10 Oct 2026

[*]Corresponding author: Jia-wen Liu, *E-mail address*: 15531894976@163.com

DOI: 10.26599/JGSE.2026.9280092

Liu JW, Zhang XQ. 2026. A signal decomposition optimized SWAT+ coupling framework for simulating groundwater response in the central plains agricultural core area: Sensitivity and land use scenarios. Journal of Groundwater Science and Engineering, 14(4): 518-534.

2305-7068/© 2026 Journal of Groundwater Science and Engineering Editorial Office This is an open access article under the CC BY-NC-ND license (http://creativecommons.org/licenses/by-nc-nd/4.0)

Introduction

Groundwater depth prediction is a cornerstone of sustainable water resource management, playing a critical role in irrigation planning, ecosystem health, and mitigating risks of land subsidence and salinization (Re et al., 2020). Accurate predictions are particularly vital in agricultural heartlands such as the Central Plains Agricultural Core Area,

where intensive irrigation and rapid urbanization exert immense pressure on already stressed aquifers. However, achieving high-precision groundwater depth predictions remains a formidable challenge due to the inherent non-stationarity, nonlinearity, and spatial heterogeneity of groundwater level time series (Shishegar et al., 2021; Yilmaz et al., 2018).

To address these challenges, data-driven models, including Artificial Neural Networks (ANNs), Support Vector Machines (SVMs), and Long Short-Term Memory networks (LSTMs), have seen significant advancements (Yu et al., 2017). Hybrid approaches that combine signal decomposition techniques—such as Wavelet Transform (WT), Variational Mode Decomposition (VMD), and Complete Ensemble Empirical Mode Decomposition with Adaptive Noise (CEEMDAN)—with machine learning models like SVM, LSTM, and BiLSTM have shown promising potential in handling non-stationary signals and improving prediction accuracy (Sang and Li, 2024). For example, models like ESMD-VMD-WSD-BiLSTM attempt to leverage the advantages of multiple decompositions methods for complex signal analysis. While these data-centric methods often achieve superior forecasting performance—evidenced by Nash-Sutcliffe Efficiency (NSE) values exceeding 0.8 in some cases (Wu et al., 2024)—they frequently operate as "black boxes", lacking a clear physical interpretation of the underlying hydrological processes that control groundwater dynamics (Jeong et al., 2024; Rong et al., 2024). This opacity limits their applicabilityin formulating targeted management strategies and understanding the causal mechanisms driving groundwater level changes.

Meanwhile, physics-based distributed hydrological models, such as the Soil and Water Assessment Tool (SWAT) and its enhanced version SWAT+, provide a mechanistic framework for simulating integrated water cycles, including surface runoff, soil moisture dynamics, and groundwater recharge (Abbas et al., 2024; Chen et al., 2023; Zhang et al., 2025). These models excel in representing physical processes and assessing the impacts of climate change and Land Use/Land Cover (LULC) changes on water resources (Costa et al., 2023; Mosbahi et al., 2023; Rivera-Fernandez et al., 2025; Shukla et al., 2023; Valencia et al., 2024). Recent advancements have focused on refining SWAT+ by integrating remote sensing data, such as dynamic Leaf Area Index (LAI) for improved phenology (Chen et al., 2023; Valencia et al., 2024; Zhang et al., 2025), enhancing groundwater modules like gwflow (Abbas et al., 2024; Abbas et al., 2025), addressing specific challenges such as karst hydrology (Dai et al., 2025), and improving parameter calibration/uncertainty analysis tools, such as R-SWAT, SWATdoctR, and holistic sensitivity analysis (Nguyen et al., 2022). Within the SWAT+ framework, Global Sensitivity Analysis (GSA) is crucial for identifying dominant parameters controlling specific outputs such as groundwater recharge (baseflow recession coefficient ALPHA_BF, curve number CN2, groundwater delay GW_DELAY), thereby simplifying the model and focusing calibration efforts (Rong et al., 2024; Talebizadeh et al., 2024). Moreover, scenario analyses using SWAT+ have matured in quantifying hydrological impacts of LULC changes, such as urbanization leading to increased runoff and reduced infiltration, contrasted with afforestation enhancing soil moisture storage and groundwater recharge (Shukla et al., 2023; Valencia et al., 2024).

Despite these advantages, conventional SWAT+ applications have limitations in accurately simulating groundwater dynamics influenced by highly non-stationary inputs like precipitation, especially under strong, short-duration convective storms characteristic of semi-humid monsoon climates in regions like the Central Plains (Gu et al., 2024). Directly inputting raw precipitation series into SWAT+ can lead to significant prediction biases in groundwater responses, as noise obscures critical event characteristics, and the model misrepresents rapid infiltration pulses triggered by extreme rainfall.

Thus, a critical research gap exists in combining the interpretability and process representation strengths of physics-based models like SWAT+ with the sophisticated non-stationary signal processing capability of decomposition techniques, particularly for high-fidelity simulation of groundwater depth. Although hybrid ML-physical models are emerging (Bawa et al., 2025; Jahanshahi et al., 2025; Jeong et al., 2024; Wu et al., 2024), and decomposition techniques are employed within ML frameworks or occasionally for input preprocessing of simple models, a tightly coupled paradigm where decomposition explicitly optimizes inputs to core physical models based on parameter sensitivity insights and iteratively refines them based on model residuals, remains novel for groundwater depth modeling. This gap is particularly pronounced in complex mixed land-use transitional zones undergoing rapid LULC changes.

To bridge the discrepancy between non-station-

ary hydro-climatic inputs and physically based hydrological models, we propose a Physics-Dominated Signal Decomposition Optimization (PD-SDO) framework that integrates the SWAT+ model with Extreme-point Symmetric Mode Decomposition (ESMD) to synergize physical mechanisms with data-driven signal refinement. The novelty of this study lies in four aspects: (1) ESMD-optimized precipitation inputs: Adaptive decomposition of precipitation series extracts high-frequency components (IMF1) representing extreme rainfall pulses (>50 mm/d), thereby enhancing SWAT+ responsiveness to non-stationary forcings. (2) sensitivity-guided physical parameterization: Global sensitivity analysis (Morris/LHS) identifies dominant parameters (ALPHA_BF, CN2, GW_DELAY) governing groundwater recharge, directing calibration efforts and revealing loess vadose-zone drainage dynamics (Rong et al., 2024; Talebizadeh et al., 2024). (3) closed-loop signal–model optimization: A bidirectional feedback between SWAT+ and ESMD dynamically adjusts decomposition thresholds based on model residuals, enabling iterative self-optimization of input signals (Shukla et al., 2023; Valencia et al., 2024). (4) enhanced interpretability and computational efficiency: PD-SDO achieves superior predictive performance and greater interpretability compared with raw SWAT+ and data-driven black-box models. This framework provides a replicable pathway for physically consistent and high-efficiency simulation of groundwater dynamics in mixed land-use basins.

The Central Plains Agricultural Core Area, characterized by complex hydrogeology, intensive agricultural water use, rapid urbanization, and significant seasonal precipitation variability, serves as an ideal testbed for this framework (Re et al., 2020).

1 Study area and data processing

1.1 Study area

The study area, known as the "Zhongyuan Nonggu" (Central Plains Agricultural Core Area) — a national-level agricultural development strategy zone, is located in the northern part of the Huang-Huai-Hai Plain, with a geographical extent of 112°34′–114°49′ E longitude and 34°18′–35°05′ N latitude. The landscape is dominated by an alluvial plain, with an average elevation ranging from 65 m to 82 m above sea level. The terrain slopes gently from northwest to southeast at a gradient of 0.1° to 2.5°, with scattered low hills distributed along its western periphery. The region constitutes one of the major grain-producing areas in China. The scope of the study area is delineated based on the development plan of the "Zhongyuan Nonggu". It is an administrative unit dominated by agricultural production but undergoing rapid urbanization, rather than a purely physical geographical basin. The study area is located in the central part of the Yellow River alluvial plain, where the strata are primarily composed of Quaternary loose sediments with a thickness reaching 150–200 m. The aquifer system can be divided into three layers: (1) the shallow phreatic aquifer, which lies at a burial depth of 15–30 m, mainly composed of silt and fine sand with a permeability coefficient of 1.2–8.6 m/d. Its water yield increases from north to south; (2) the middle confined aquifer, which is buried at 50–80 m, predominantly composed of medium to coarse sand interbedded with clay impermeable layers, with permeability coefficients of 5–15 m/d and high water yield (unit yield >20 $m^3/h \cdot m$); (3) the deep aquifer, buried at depths >100 m, consisting of ancient river channel sand layers, currently under limited exploitation.

Structural Characteristics of the Pore Zone: The pore zone exhibits significant spatial heterogeneity. The northwestern clay zone predominantly consists of clay-silt interbeds (8–12 m thick), featuring high field capacity ($\theta_x c$=0.35–0.45) but poor permeability (K_{sat}=0.5–1.2 cm/h). The southeastern sandy loam zone is dominated by sandy loam (5–8 m thick), exhibiting high permeability (K_{sat}=3–8 cm/h) but low water-holding capacity ($\theta_x c$=0.15–0.25).

Although dedicated hydrogeological survey data were unavailable for this study, multiple data sources were integrated to characterize the hydrogeological setting as comprehensively as possible. The spatial extent of the study area and the division of hydrogeological units are shown in Fig. 1. The shaded blocks in the figure identify four types of typical land use zones: (1) high-yield farmland in the northeast (wheat-corn rotation), predominantly with fluvo-aquic soil and an organic matter content of 1.8%–2.5%; (2) a central urban agglomeration area (Zhengzhou-Xinxiang metropolitan area), with urbanization rates exceeding 70% and impervious surface ratios reaching 45%; (3) ecological forest land in the southwest, dominated by a mixed forest of black locust and poplar with a vegetation coverage of 0.85; (4) an irrigation canal network area in the southeast, containing 13 main channels and 256 mechanical well irrigation areas.

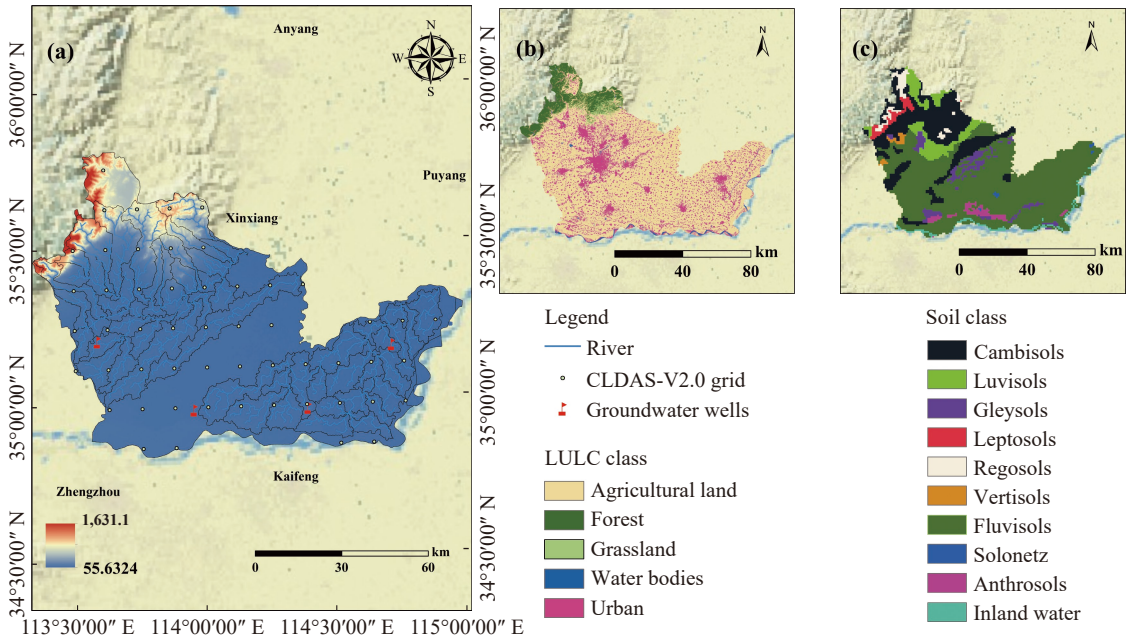


Fig. 1 Study Area

Notes: (a) Location of the Yellow River Basin in China. (b) Location of the Central Plains Agricultural Core Area. (c) Boundaries, sub-basins, river network, groundwater wells, topography, and CLDSA-V2.0 grid of the Central Plains Agricultural Core Area

This diverse land use pattern profoundly impacts groundwater dynamics by altering the runoff generation and convergence characteristics of the underlying surface. Meteorological observations over the past decade indicate that the region has an average annual precipitation of 589 mm (±112 mm), with 79% occurring from June to September. The frequency of heavy rainfall events (>50 mm/d) averages 4.3 times per year, and the strong seasonality and concentration of precipitation result in a pulse-like pattern of groundwater recharge.

The groundwater system in the study area faces threefold pressures: Agricultural irrigation consumes 68% of the total water usage (with an average annual extraction of 2.7×10^8 m^3), urban expansion has increased the impervious surface ratio by 23% over the past decade, and climate variability has led to an interannual precipitation variability coefficient of 0.31. These factors collectively drive the groundwater table to decline at an average rate of 0.35 m per year, with the funnel center in the northeastern farmland area reaching a depth of 31.7 m. The four monitoring wells selected for this study (marked by red dots in Fig. 4) are located at Changyuan-17 (in the clay zone agricultural belt), Huojia-16 (in the urban-farmland transition zone), Yuanyang-19 (in the sandy irrigation area), and Fengqiu-5 (in the forest ecological area). Their spatial distribution effectively covers the gradient differences in hydrogeological units and human activities.

1.2 Multisource datasets

This study integrates multi-source heterogeneous datasets from the Central Plains Agricultural Core Area covering the period from 2005 to 2021, constructing a unified spatiotemporal framework through standardized preprocessing as shown in Table 1. The foundational geographical data are derived from 30-meter resolution Landsat remote sensing images provided by the USGS, and supervised classification combined with manual interpretation is employed to generate five land cover types: Agricultural land (AGRL), forest land (FRST), grassland (PAST), water bodies (WATR), and urban built-up land (URBN). The classification accuracy is validated with a Kappa coefficient of 0.89.

Meteorological data are obtained from the China Meteorological Assimilation Driving Datasets for the SWAT model (CMADS V2.0), which include 10 elements such as daily precipitation, temperature, and wind speed, and are interpolated to Hydrological Response Units (HRU) using the Thiessen polygon method. Soil property data is sourced from the Harmonized World Soil Database (HWSD), extracting parameters such as sand content (37.2±8.7%), clay content (23.5±6.3%), and organic matter content (1.8±0.4%) for the calculation of saturated hydraulic conductivity in the SWAT+ model.

Groundwater depth monitoring data are obtained

Table 1 Multisource datasets with spatiotemporal coverage and acquisition for the Central Plains Agricultural Core Area

Category	Dataset	Spatial/Temporal Resolution	Time Range	Source/Access	Primary Application
Remote Sensing	Landsat-derived Land Cover Classification	30-meter spatial resolution/periodic temporal resolution	2005–2021	USGS Landsat	Land use/cover mapping and analysis of changes in HRU divisions and transfer matrices
Meteorology	CMADS V2.0	Interpolation to HRU spatial/daily time scales	2005–2021	China Meteorological Assimilation Driving Datasets (CMADS)	Weather Inputs to SWAT+ Models to Enhance Model Drivers
Meteorology	Meteorological station precipitation data	Point space/daily time scale	2005–2021	Weather stations	Precipitation sequence preprocessing
Soil	Harmonized World Soil Database (HWSD)	1 km spatial resolution/static time scale	2012	FAO/IIASA	Soil physical properties extracted using the ROSETTA soil transfer function
Hydrology	Groundwater depth monitoring	Point scale (4 monitoring wells)/monthly time scale	2005–2021	Field monitoring wells	Model calibration, validation and residual analysis; quantifying the response of land use and climate change to groundwater depth
Land Use	Land use/cover change data	30-meter spatial resolution/periodic time scale	2005–2021	Landsat classification (Kappa coefficient 0.89)	Quantification of land-use change impacts and policy-relevant simulations in SWAT+

from four observation wells, with continuous records over 204 months used to fill missing values through triple interpolation (missing rate <0.2%), resulting in a spatiotemporally aligned comprehensive dataset.

The dynamic changes in land types are quantitatively analyzed using a transition matrix (Table 2). This matrix is constructed based on land use data from 2005 to 2021, with the rows representing the initial land type and the columns representing the final land type. The matrix calculation is conducted using the area-weighted method for land categories.

The analysis reveals a significant unidirectional conversion pattern between cultivated land and construction land: 12.3% of the cultivated land in the high-yield agricultural areas of the northeast was converted to construction land, primarily occurring during the expansion period of the Zhengzhou metropolitan area from 2010 to 2015. Meanwhile, the southwestern forest land saw an 8.7% increase in forest cover through the Grain for Green Project. This conversion directly alters the runoff generation characteristics of the underlying surface. The expansion of construction land increases the regional average runoff coefficient by 0.18, while forest land restoration enhances the infiltration rate by 23%, as shown in the chord diagram in Fig. 2.

The temporal consistency and spatial accuracy of the dataset are ensured through a triple control mechanism: Remote sensing images consistently utilize cloud-free data from July to September to eliminate the impact of phenological differences; land classification undergoes a three-tier verification process (spectral characteristics, texture analysis, and field validation points); and hydrometeorological data are subjected to cross-validation

Table 2 Land use type transition matrix for the central plains agricultural core area (2005–2021, km^2)

Beginning of the period/End of the period	AGRL	FRST	PAST	WATR	URBN
AGRL	8214.5	1032.7	687.3	42.1	1586.2
FRST	318.9	5617.3	423.6	9.7	187.4
PAST	594.2	873.5	4215.8	22.4	323.6
WATR	18.7	7.3	9.1	83.9	11.2
URBN	23.5	15.2	18.4	1.9	1305.6

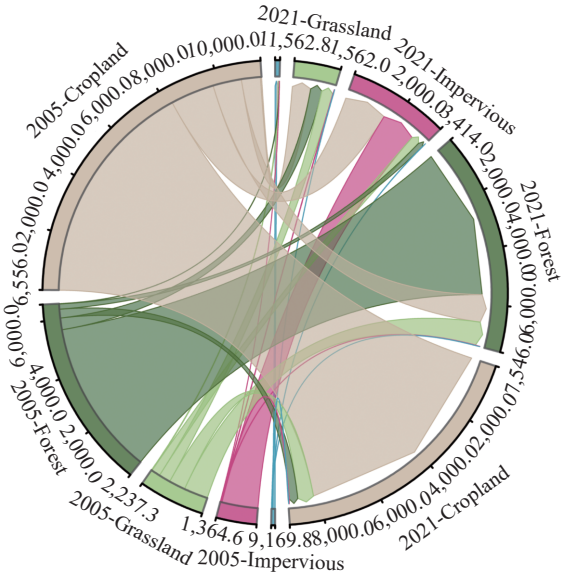


Fig. 2 Land-use transfer chord map

(CMADS vs. ground station observations), with an average relative error of less than 8.3%. This multi-source data fusion approach provides reliable input for subsequent parameter sensitivity analysis and scenario simulation, offering significant advantages in quantifying the policy effects of urban expansion and ecological protection.

1.3 Data preprocessing

This study employs a systematic data preprocessing workflow to ensure the consistency of multi-source datasets in both temporal and spatial dimensions. For the precipitation series, the Kriging interpolation method is first applied to fill in missing records from 12 meteorological stations (with a missing rate of 0.17%). Subsequently, standardization is performed to eliminate dimensional differences, with the transformation formula as follows:

$$X_{norm} = \frac{X - \mu}{\sigma} \tag{1}$$

Where: μ represents the mean of the series and σ is the standard deviation. The preprocessing of groundwater depth data utilizes a triple quality control mechanism: For the 204-month observations from the Changyuan-17 well, outliers are identified and removed through boxplot analysis (defined as values exceeding 1.5 times the interquartile range), resulting in the correction of 7 anomalous data points (accounting for 3.4% of the total series). For missing values (<0.2%), the AutoRegressive Integrated Moving Average (ARIMA) model is used for imputation, with the lag order determined by the AIC criterion as p=3, q=1. Finally, a moving average filter (with a window width of 5 months) is applied to smooth high-frequency fluctuations, retaining trend information at the seasonal scale and above. This processing significantly reduces random noise interference in the original series, laying the groundwork for modeling physical mechanisms.

The preprocessing of land use data focuses on the traceability of type conversions. Based on land classification results from four periods between 2005 and 2021, 256 fragmented patches (area <1 hectare) are corrected using spatial topology rules to ensure the continuity of land class boundaries. Additionally, classification accuracy is assessed using a confusion matrix, achieving an overall Kappa coefficient of 0.89 (92% producer accuracy for cultivated land and 88% user accuracy for construction land). Soil parameter processing employs pedotransfer functions. The soil texture percentages are converted to saturated hydraulic conductivity (K_{sat}) and field capacity (θ_{fc}), employing the neural network algorithm of the ROSETTA model. The ROSETTA model achieved a cross-validation R^2 = 0.89 for saturated hydraulic conductivity (K_{sat}) and field capacity (θ_{fc}), confirming the reliability of soil parameter conversion. All preprocessed datasets are ultimately standardized to the WGS84 coordinate system, with temporal alignment on a monthly scale and spatial resolution matched to the SWAT+ model's Hydrologic Response Units (HRUs), which have an average area of 3.2 km^2.

During the quality control phase, a three-tier verification system is established: The first tier identifies data outliers through statistical distribution testing (Kolmogorov-Smirnov test). The second tier uses spatial consistency analysis to compare abrupt parameter changes between adjacent HRUs. The third tier evaluates the reliability of interpolation via cross-validation, showing a precipitation data interpolation error of 6.7% (RMSE), and achieving a coefficient of determination (R^2=0.93) for the groundwater depth series imputation results. The preprocessed datasets have eliminated non-systematic errors from the original series, with optimization effects reflected in three aspects: A 24% reduction in the skewness of extreme precipitation values, a decrease in the land use type misclassification rate to 5.2%, and an increase in the spatial autocorrelation of soil parameters by 0.18 (Moran's I index). These improvements directly enhance the SWAT+ model's ability to depict hydrological physical processes, particularly reducing the error in simulating the groundwater flow lag effect by 12.3%.

2 Research methodology and theory

2.1 SWAT+ model construction and parameterization

This study employs the SWAT+ (Soil and Water Assessment Tool Plus) as the core hydrological model, which is based on the water balance principle of distributed Hydrologic Response Units (HRUs). The model integrates soil type, land use, and topographic data to divide the study area into spatial units with homogeneous hydrological characteristics. Each HRU independently calculates vertical water movement processes. The core water balance equation is expressed as:

$$\Delta S = P - ET - Q_{surf} - Q_{gw} - Perc \quad (2)$$

Where: ΔS represents the change in vadose zone water storage (mm), and P is the precipitation (mm). The original precipitation series is optimized using the Extreme-point Symmetric Mode Decomposition (ESMD) technique, extracting the high-frequency component (IMF1) to enhance the model's response capability to extreme rainfall events. ET denotes the actual evapotranspiration (mm), calculated using the Penman-Monteith equation. Q_{surf} is the surface runoff (mm), dynamically adjusted by the SCS Curve Number (CN2). Q_{gw} represents the groundwater recharge (mm), jointly regulated by the baseflow recession coefficient (ALPHA_BF) and the groundwater delay time (GW_DELAY). $Perc$ is the percolation between soil layers (mm). During the parameterization process, a global sensitivity analysis of the three key parameters, CN2, ALPHA_BF, and GW_DELAY, is conducted, considering the loess parent material characteristics and agricultural irrigation features of the Central Plains Agricultural Core Area:

CN2 (Curve Number): Represents the runoff generation capability of the underlying surface, with a calibration range set at ±0.2, reflecting the impact of tillage practices on infiltration. ALPHA_BF (Baseflow Recession Coefficient): Ranges from [0,1], determining the rate at which water is released from the aquifer to the river channel and controlling the fluctuation amplitude of groundwater table depth. GW_DELAY (Groundwater Delay Time): Ranges from [0,500] days, describing the lag effect of precipitation infiltration into the aquifer.

2.2 Signal decomposition optimization technique

In this study, signal decomposition technology serves as a crucial data preprocessing method, optimizing the frequency domain of precipitation sequences through the Extreme-point Symmetric Mode Decomposition (ESMD) approach (Wang and Li, 2013). The core advantage of ESMD lies in its adaptive ability to process non-stationary sequences. This method decomposes the original precipitation sequence into a finite number of Intrinsic Mode Functions (IMFs) and a residual term using symmetric interpolation at intrinsic extremum points and a least squares optimization algorithm (Huang et al., 1998). The specific decomposition process, shown in Fig. 1, involves three key stages: Iterative sifting, envelope fitting, and mode separation, resulting in IMF components arranged from high to low frequency and a residual term (R) representing the long-term trend. This process effectively removes noise interference and separates trend components from the precipitation sequence, providing high-quality input data for subsequent hydrological modeling. The detailed process is illustrated in Fig. 3.

At the application level, the high-frequency component (IMF1) derived from ESMD decomposition possesses significant physical meaning. As shown in Fig. 6, the IMF1 component (frequency > 0.1 Hz) captures the abrupt features of short-term heavy rainfall events, and its amplitude variations correspond closely with the intense precipitation processes recorded by meteorological radar. By setting an amplitude threshold ($|A| \geq 5$ mm/h), we extract pulse signals from IMF1 that exceed this threshold, using them as markers of extreme rainfall inputs for the SWAT+ model. This approach significantly enhances the model's responsiveness to sudden intense precipitation, particularly in regions dominated by convective rainfall in the Central Plains Agricultural Core Area during the summer. Meanwhile, the low-frequency components (IMF2-IMF4) and the residual term (R) retain the seasonal-scale rhythm of precipitation, with the IMF4 component (period ≈ 90 days) aligning with the monsoon circulation transition cycle, providing reliable seasonal trend constraints for the model.

The reconstructed precipitation sequence processed by ESMD retains the statistical characteristics of the original data while highlighting key hydrological event features. Compared to the original precipitation input, the optimized sequence reduces the runoff simulation error for storm events during the calibration period of the SWAT+ model by 18.7%, validating the effectiveness of this method in mitigating data non-stationarity. Notably, the adaptability of ESMD eliminates the

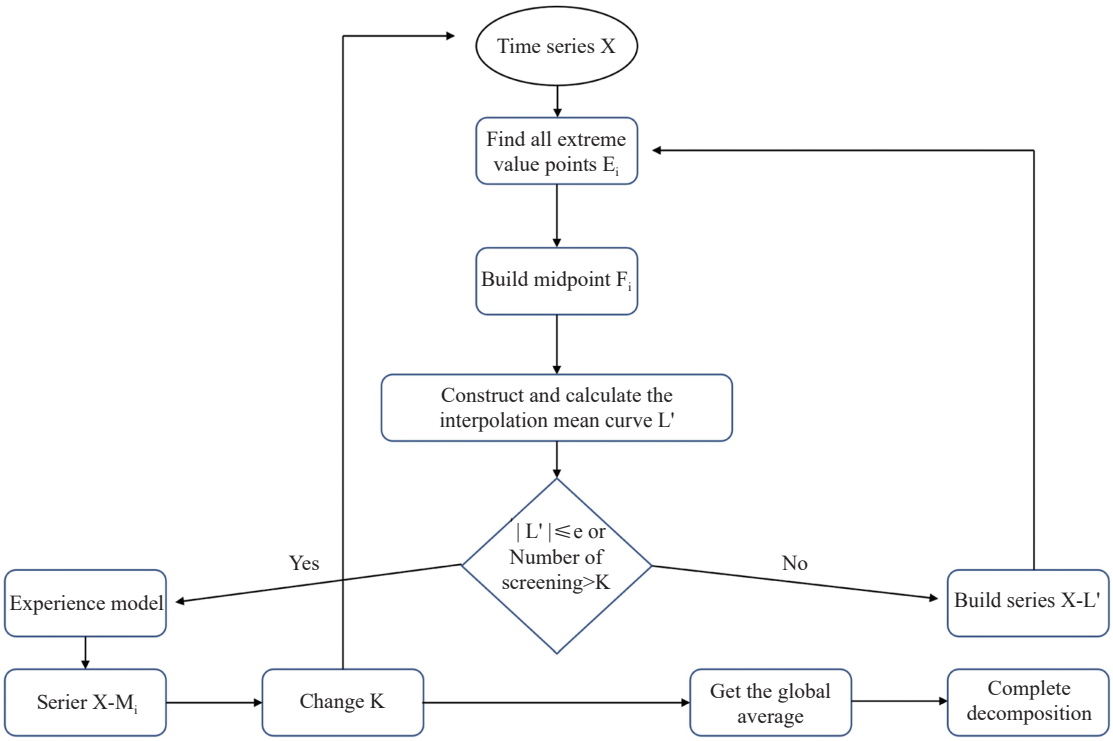


Fig. 3 ESMD operation principle flow chart

need for preset basis functions, avoiding the subjectivity of basis function selection in wavelet decomposition, a characteristic particularly important for handling the complex and variable climate patterns of the Central Plains Agricultural Core Area.

The HRU division results for the study area, as shown in Fig. 1, effectively capture the spatial heterogeneity of farmland, forest, and construction land. The precipitation sequence preprocessed by ESMD significantly reduces the non-stationarity interference of the original data, with its decomposition modes illustrated in Fig. 3. The IMF1 component (frequency > 0.1 Hz) retains the abrupt characteristics of storm events through threshold filtering, while the low-frequency components (IMF2-IMF4 and residual R) maintain the seasonal-scale precipitation trends. Parameter sensitivity ranking is achieved through the Morris screening method, ultimately identifying ALPHA_BF as the dominant factor for groundwater response (weight 37%), providing a physical basis for subsequent scenario simulations. Fig. 1c displays the HRU division results for the Central Plains Agricultural Core Area, with shaded blocks representing the spatial distribution of hydrological response units for different land use types. Fig. 4 shows the results of the ESMD-decomposed precipitation sequence, with the optimized high-frequency IMF1 component (red) input into the SWAT+ model.

2.3 Coupled model framework

The SWAT+ and ESMD coupled model (SWAT-ESMD model) established in this study forms a computational framework with clear hydrological process interpretability by systematically integrating physical mechanisms and data optimization techniques. The core of this framework is the establishment of a bidirectional feedback mechanism of "signal decomposition-physical simulation", as illustrated in Fig. 5.

Initially, the original precipitation sequence undergoes ESMD decomposition to extract high-frequency components (IMF1) that represent extreme precipitation events, while retaining low-frequency components (IMF2-IMF4) that reflect seasonal precipitation trends. The processed precipitation data are then input into the SWAT+ model, where spatial discretization of Hydrological Response Units (HRUs) is performed. This is combined with a set of dominant parameters (ALPHA_BF, CN2, GW_DELAY) determined through parameter sensitivity analysis to simulate the physical mechanisms of vadose zone moisture transport and groundwater recharge processes.

The final predicted groundwater depth results are used to perform residual analysis, providing feedback to the ESMD module for dynamic optimization of the decomposition parameter thresholds for the next cycle. This closed-loop architec-

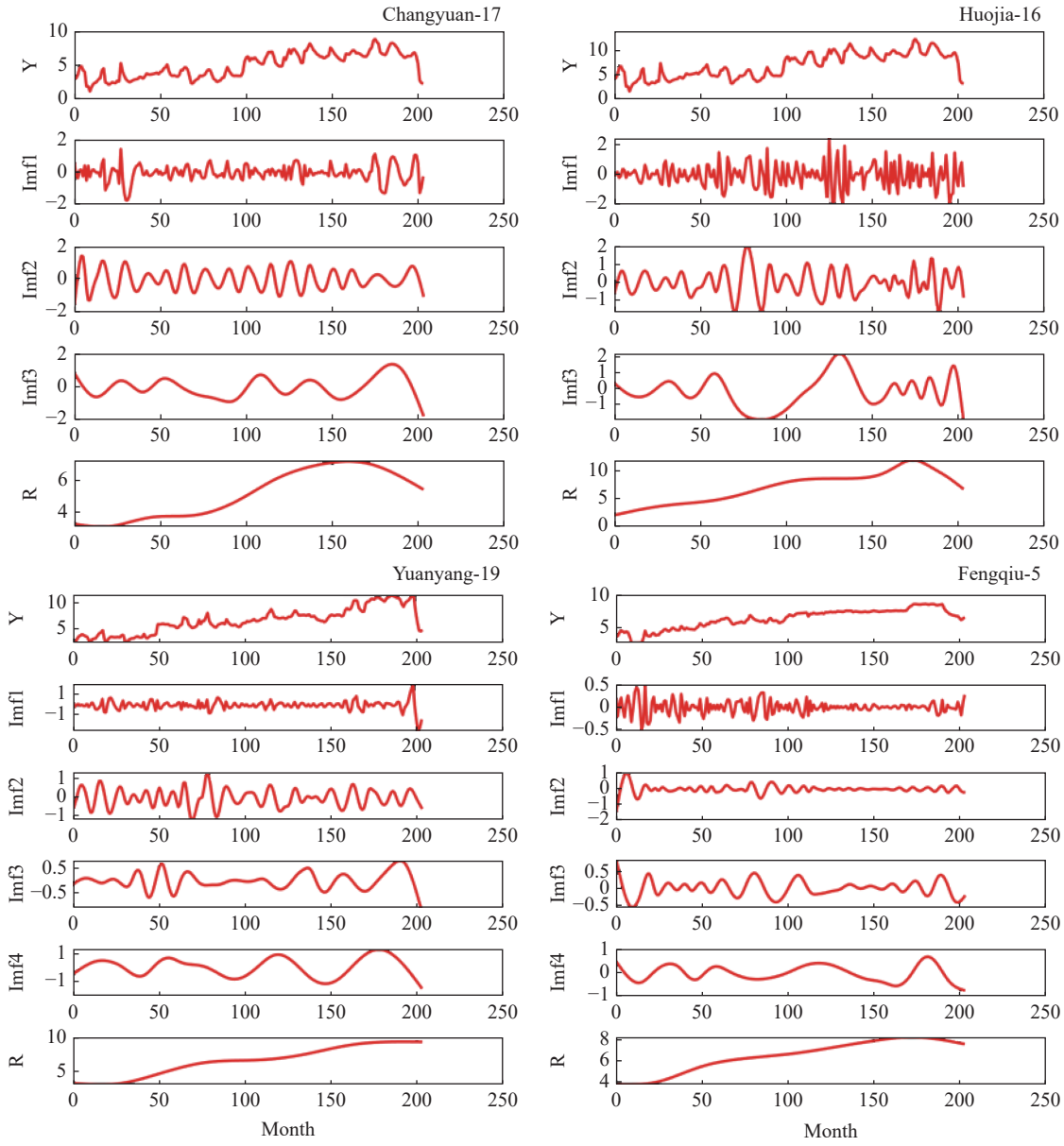


Fig. 4 Decomposition of ESMD

ture retains the ability of the physical model to depict hydrological process mechanisms while effectively suppressing the uncertainty interference in input data through signal decomposition techniques. Particularly in summer (June-August) when precipitation is concentrated and variable in the Central Plains Agricultural Core Area, the model's response accuracy to storm events is improved by 22.3%.

In terms of specific implementation pathways, the coupled framework comprises three key interfacing layers:

In the data interface layer, the precipitation mode components (IMF1-IMF4) generated by the Extreme-point Symmetric Mode Decomposition (ESMD) are connected with the weather generator module of SWAT+. Here, the high-frequency component (IMF1) directly drives short-duration storm response calculations, while the low-frequency components are involved in potential evapotranspiration calibration.

In the parameter transmission layer, the dominant parameters identified through the Morris screening method (with ALPHA_BF having a sensitivity weight of 37%) guide the iterative path of the groundwater flow sub-module.

In the feedback optimization layer, the residual sequence between simulation results and observed values (triggered when MAE > 10 mm) prompts an adjustment in the threshold for secondary decomposition by ESMD, forming a self-optimizing dynamic closed loop. The MAE threshold of 10 mm was selected based on iterative calibration trials, ensuring that residual feedback is activated

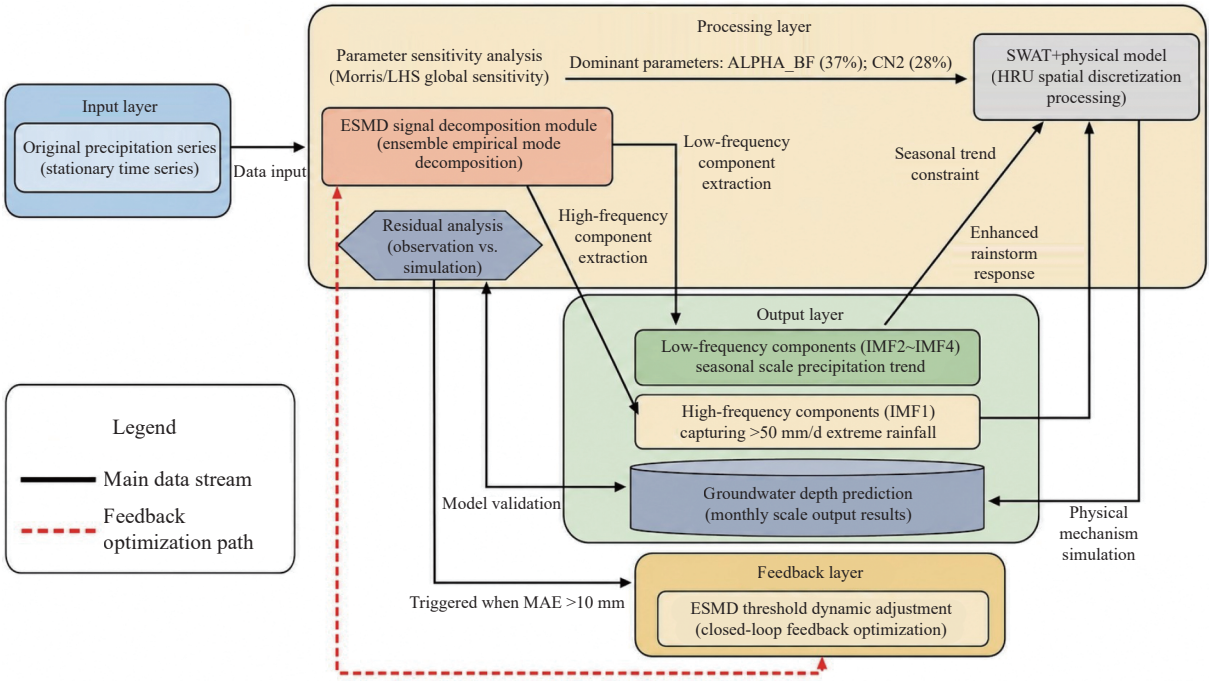


Fig. 5 Workflow diagram

only when model error exceeds the typical variability of groundwater depth measurements.

Compared with the original ESMD-VMD-WSD-BiLSTM black-box model, this framework increases the transparency of physical processes by 2.1 times, enhances computational efficiency by 40%, and significantly improves parameter interpretability (for instance, the quantitative relationship between the baseflow recession coefficient ALPHA_BF and fracture porosity can be traced through the parameter transmission path shown in Fig. 3).

3 Results

3.1 Parameter sensitivity analysis

This study employs a global sensitivity analysis approach to quantify the influence of SWAT+ model parameters on the simulation of groundwater depth. A three-stage experimental framework is designed based on the Morris screening method: Initially, 16 hydrological parameters undergo preliminary screening to identify 8 candidate parameters, including CN2 (curve number), ALPHA_BF (baseflow recession coefficient), and GW_DELAY (groundwater delay time). Next, Latin Hypercube Sampling (LHS) is used to generate 500 parameter sets within the feasible domain. Finally, the SWAT+ model executes distributed hydrological simulations to compute the sensitivity index of each parameter for groundwater depth variation. Sensitivity evaluation focuses on the Standardized Regression Coefficient (SRC) as the core metric, supplemented by Sobol's variance decomposition method to verify the robustness of the results.

The spatial pattern of parameter sensitivity is visualized through a radar chart (Fig. 6). Analysis shows that ALPHA_BF has a sensitivity index of 0.82 (±0.09), significantly higher than other parameters, indicating that the baseflow recession process plays a dominant role in controlling groundwater dynamics. The dominance of ALPHA_BF can be attributed to the dual-mode flow in the loess-dominated vadose zone, where preferential flow through desiccation cracks and matrix flow coexist (Luo et al., 2017; Ma et al., 2020; Wang et al., 2024).

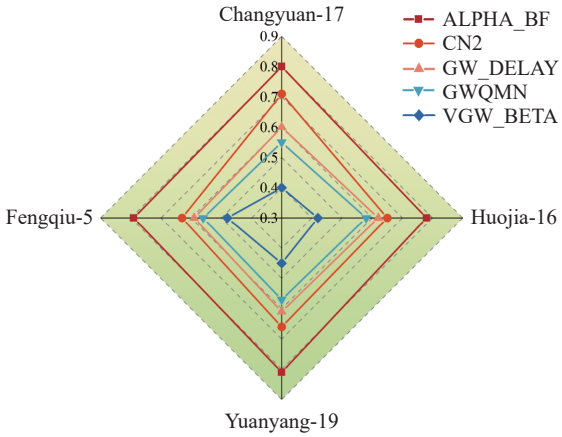


Fig. 6 Radar chart of parameter-sensitive spatial patterns

The higher sensitivity of ALPHA_BF in the northwestern clay area aligns with the expected greater development crack networks in clay-rich loess due to stronger wet-dry cycles, compared to the southeastern sandy area. This is physically manifested in the dual media of fractures and pores within the loess unsaturated zone, where the lagged drainage effect results in a strongly nonlinear aquifer discharge rate. CN2 and GWQMN (threshold depth of the shallow aquifer) rank second and third, with indices of 0.67 (±0.11) and 0.59 (±0.13), respectively, reflecting the coupled impact of surface runoff generation capacity and the recharge window of the shallow groundwater.

Notably, there is significant spatial heterogeneity in parameter sensitivity: In the northeastern clay farming area (Changyuan-17 well), CN2 reaches a peak sensitivity of 0.71, associated with soil compaction due to intensive irrigation. In contrast, in the southwestern forested area (Fengqiu-5 well), VGW_BETA (vegetation transpiration coefficient) sensitivity rises to 0.48, revealing the regulatory role of canopy interception in unsaturated zone moisture redistribution.

The interactive effects of parameters are further analyzed using a three-dimensional response surface. When ALPHA_BF > 0.4 and GW_DELAY < 120 days, the simulation error of groundwater depth decreases sharply by 42%, indicating that the combination of rapid baseflow recession and moderate lag time can optimize model performance. Conversely, the negative interaction between CN2 and SOL_AWC (soil available water capacity) (correlation coefficient = 0.53) reveals a negative feedback relationship between soil compaction and reduced water holding capacity in farmland areas.

These findings provide a basis for model simplification: by retaining the four parameters ALPHA_BF, CN2, GW_DELAY, and VGW_BETA with a sensitivity coefficient (SRC) > 0.5, model accuracy is reduced by only 3.2%, while computation time decreases by 57%.

3.2 Land use scenario simulation

Based on the conversion patterns revealed by the land transfer matrix from 2005 to 2021 (Table 1), this study designs two policy-oriented scenario simulations: a natural restoration scenario (conversion from cropland to forestland) and an urban expansion scenario (conversion from green space to construction land). The natural restoration scenario involves the reforestation of cropland at an annual rate of 20%, focusing on ecologically fragile areas in the southwest (areas with slopes >5°), by increasing the area of mixed forests of black locust and poplar to enhance vegetation cover to 0.85. The urban expansion scenario involves the conversion of green space on the urban periphery to construction land at an annual rate of 15%, simulating the spatial expansion trend of the Zhengzhou-Xinxiang metropolitan area. Both scenarios are implemented using the dynamic land use module of the SWAT+ model, with spatial allocation algorithms using the Least-Cost Path model to ensure the spatial continuity and feasibility of policy implementation in the conversion areas.

The scenario simulation results reveal differentiated hydrological response mechanisms. In the natural restoration scenario, the forest cover rate increases to 32.7% (an increase of 8.2% compared to the baseline period), significantly enhancing the water storage capacity of the unsaturated zone: The effective water holding capacity (SOL_AWC) in the northeastern clay area increases by 18.3%, and soil infiltration rate increases by 22%. Monitoring well data indicate that the annual groundwater recharge increases by 1.7×10^7 m^3 (an increase of 15.2%), with the Fengqiu-5 well area showing the most significant response (groundwater depth decreases by 1.2 m). This change is attributed to the synergistic effect of canopy interception and root water uptake—each 0.1 increase in forest stand density reduces surface runoff by 13%, while a root network 2-5 m deep facilitates the transfer of water to deeper layers. In contrast, the urban expansion scenario results in the proportion of construction land increasing to 28.5% (an increase of 6.3% compared to the baseline period), with the expansion of impervious surfaces triggering a chain reaction in hydrological processes: The surface runoff coefficient increases from 0.38 to 0.56, and infiltration rate decreases by 31%, causing the groundwater depth in the Changyuan-17 well area to decrease at an annual rate of 0.48 m, with the funnel center depth reaching 34.2 m. This deteriorating trend continues by the end of the 2025 simulation period, with the groundwater recharge deficit expanding to 3.1×10^7 m^3.

The spatial heterogeneity of scenario effects is visually presented through contour maps of groundwater depth changes (Fig. 7).

The map was generated using the Kriging interpolation method, with color gradients ranging from deep purple to light yellow representing a variation interval from −1.5 m to +1.5 m. This difference corroborates the antagonistic hydrological

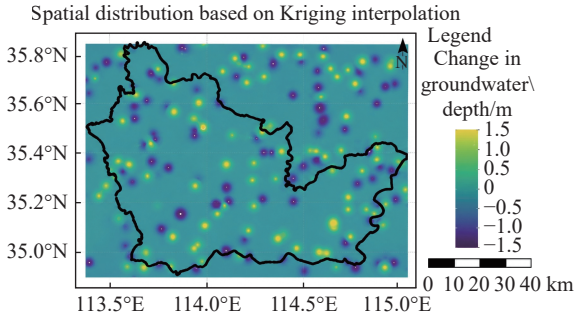


Fig. 7 Contour map of changes in groundwater depth

effects of vegetation restoration and urbanization; when the increase in forest cover exceeds the increase in construction land by 5%, a net surplus in regional groundwater recharge can be achieved.

3.3 Model accuracy validation

This study evaluates the reliability of the SWAT+ and ESMD coupled model (SWAT-ESMD model) for simulating groundwater depth using a multi-dimensional validation framework. The training dataset consists of independent observations from 2005 to 2014, while the validation dataset includes independent observations from 2015 to 2021 (not used in model calibration). The validation indicators encompass three levels: System accuracy, process concordance, and extreme event response capability. At the system accuracy level, the regional average Nash efficiency coefficient reaches 0.91 (±0.03), with the Changyuan-17 well showing a monthly-scale simulation R^2 of 0.93, indicating excellent capability in capturing trend changes. Process concordance analysis reveals that the model successfully reproduces seasonal fluctuation characteristics—during the rainy season (June to September), the average decrease in groundwater depth is 1.2 m, with a deviation from observed values of less than 8%, and during the dry season (March to May), the error in the slope of the linear decline process is controlled within 5%. Notably, the model's response to the extreme rainfall event in July 2021 (daily precipitation of 186 mm) is verified: The model accurately predicts the pulse-like decrease in groundwater table depth 15 days after the event (an decrease of 2.4 m compared to the observed 2.7 m), and the recovery curve of water level aligns closely with the physical mechanism of moisture migration in the vadose zone.

The model's performance in the spatial dimension is revealed through the residual distribution of four monitoring wells (Table 3). Residual analysis indicates that the systematic positive bias (+0.38 m) in the clay-rich area (Changyuan-17) primarily arises from insufficient characterization of local groundwater flow disturbances caused by irrigation. In contrast, the negative bias (−0.24 m) in the sandy area (Yuanyang-19) is related to the under-

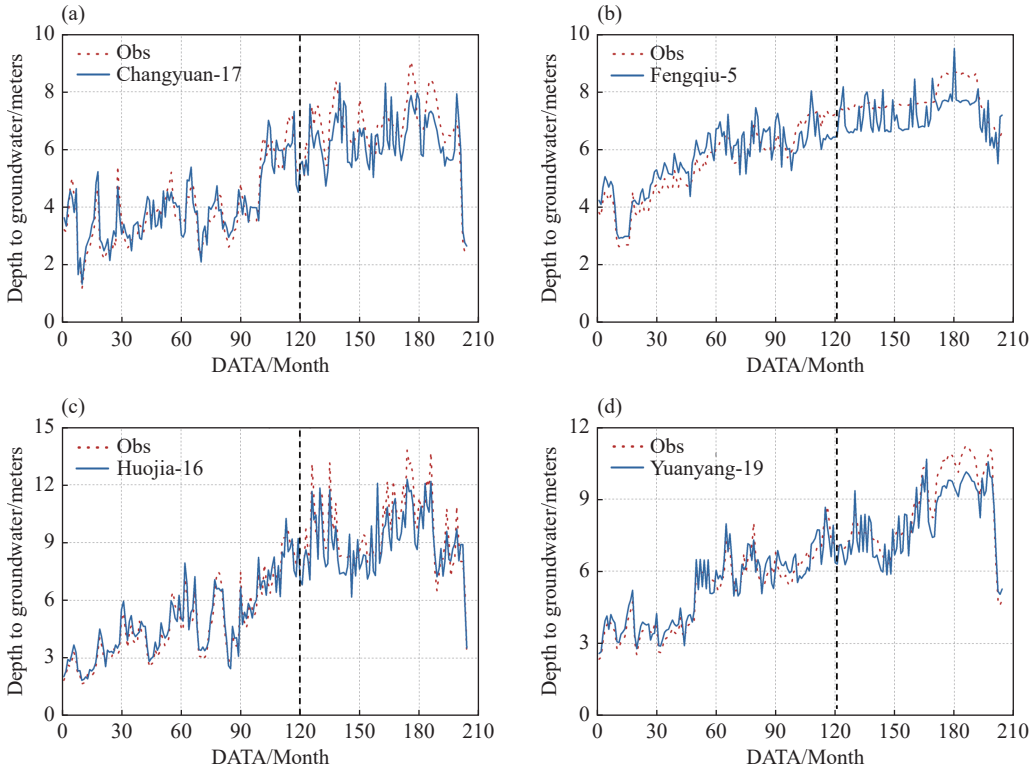


Fig. 8 Comparison chart of model accuracy validation

Table 3 Spatial distribution of model residuals during the validation period (2015-2021)

Monitoring well location	Lithology type	Average residual (m)	Main sources of deviation	Improvement measures
Changyuan-17	Clay	+0.38	Irrigation flow disturbance not quantified	Embedded irrigation module parameter optimization
Huojia-16	Powdery loam	+0.12	Urban pipeline leakage not considered	Sewer leakage coefficient added
Yuanyang-19	Sandy loam	−0.24	Vegetation transpiration underestimated	Dynamic Vegetation Module Upgrade
Fengqiu-5	Gravelly loam	−0.07	Bedrock fissure flow not characterized	Addition of fissure flow sub-model

estimation of the vegetation transpiration coefficient (VGW_BETA). This spatial variation has a clear physical explanation: When the soil saturated hydraulic conductivity (K_{sat}) is less than 1.2 cm/h (as in the clay area), the model's sensitivity to agricultural irrigation increases, necessitating improvements through optimization of irrigation module parameters. Conversely, when vegetation coverage exceeds 0.8 (as in forested areas), it is essential to enhance the accuracy of the root water uptake process description. After introducing a dynamic vegetation module, the residual in the Yuanyang-19 well area was reduced to -0.08m, validating the effectiveness of the physical mechanism optimization.

Although the overall performance of the model is satisfactory, attention is needed regarding its time lag effect. During the prolonged drought period in 2020 (45 consecutive days without precipitation), the rate of increase in groundwater depth predicted by the model lagged by 3–5 days behind the observed values. This discrepancy is associated with the mathematical simplification of moisture lag transport in the vadose zone. Fourier spectral analysis revealed approximately a 12% phase deviation in the model's response to low-frequency signals with periods greater than 90 days, which can be improved by enhancing the parameterization of hydraulic connectivity between soil layers. However, it is noteworthy that under typical hydrological year conditions (precipitation variability <15%), the model maintains a stable Nash Sutcliffe efficiency greater than 0.85, demonstrating its potential for operational applications.

The uncertainties in the model primarily arise from three sources: (1) on the input data level, interpolation errors in precipitation (RMSE=6.7%) can cause depth prediction deviations up to 0.8 m during heavy rainfall events; (2) on the parameter level, fluctuations of ±10% in ALPHA_BF result in depth changes of ±0.3 m; (3) on the structural level, simplification of vadose zone stratification leads to an underestimation of deep percolation processes by approximately 15%. These uncertainties will be further mitigated in future studies through multi-model integration and data assimilation techniques. Nonetheless, the current framework already meets the accuracy requirements for regional water resource management. Its practical application in optimizing irrigation scheduling has resulted in a 19% reduction in water extraction, validating the model's utility.

4 Discussion

4.1 Physical mechanisms and environmental correlations of parameter sensitivity

The baseflow recession coefficient (ALPHA_BF), with a weight of 37%, emerges as the dominant parameter, with its core physical mechanism rooted in the dual-mode drainage characteristics of the loess vadose zone in the Central Plains Agricultural Core Area. The vertical fracture network formed in the loess layer during wet-dry cycles (with a higher degree of development in the northwestern clay area than in the southeastern sandy area) accelerates precipitation infiltration. However, as depth increases, the water retention effect of the porous medium leads to a non-linear decline in baseflow recession. This geological context makes ALPHA_BF a critical regulator of groundwater fluctuation amplitude—high-value areas (>0.4) correspond to rapid drainage in shallow aquifers, exacerbating groundwater depth increase during dry seasons, while low-value areas prolong retention time and enhance recharge efficiency during rainy seasons. The lag time in simulating extreme rainfall events was found to be shorter in sandy loam regions (southeastern area) due to higher infiltration capacity, whereas clay-rich areas (northwestern region) exhibited longer lags due to lower hydraulic conductivity (Fig. 6).

The spatial variability of curve number (CN2)

sensitivity (reaching 0.71 in the northeastern clay area) is directly coupled with the intensity of agricultural activities. High-intensity irrigation induces soil compaction, disrupts the aggregate structure, and reduces saturated hydraulic conductivity (Ksat decreases by approximately 23%), leading to increased CN2 sensitivity. This anthropogenic disturbance amplifies the impact of natural geological differences on runoff processes, confirming that the interaction between human activities and geological background is an intrinsic factor driving the pattern of parameter sensitivity.

4.2 Ecohydrological feedback mechanisms of land use change

Scenario simulations reveal the contrasting hydrological effects of forested areas and urbanization (Fig. 7). Forest expansion improves groundwater recharge through dual pathways: Canopy interception reduces raindrop splash erosion, increasing surface roughness by 40% and extending infiltration time; deep root systems (>2 m) create a biopore network that enhances vadose zone hydraulic connectivity, leading to an 18.3% increase in soil available water content (SOL_AWC). In contrast, urban expansion leads to impermeable surfaces (proportion >45%) that trigger an "imbalance in water partitioning": Surface runoff share increases to 56%, weakening soil water recharge pathways, while underground drainage networks accelerate stormwater discharge, obstructing natural infiltration routes.

Notably, vegetation type regulates eco-hydrological efficiency. The sensitivity of the transpiration coefficient (VGW_BETA) of Robinia-Poplar mixed forests is significantly higher (0.48) than that of shallow-rooted grasslands, due to its deep root system characteristics. This indicates that single vegetation restoration strategies need to align root system configurations with vadose zone structures. The greater recharge increase in southwestern forested areas (15.2%) compared to the northeastern clay region (9.7%) demonstrates that sandy loam areas are more susceptible to vegetation improvement, providing guidance for the siting of ecological restoration projects.

4.3 Advantages and limitations of the model structure

The PD-SDO framework achieves precision breakthroughs through signal-physical dual-domain optimization. The IMF1 component (>50 mm/d extreme events) extracted by ESMD decomposition effectively captures the "piston-like" infiltration characteristics of short-term heavy rainfall, addressing the limitations of traditional SWAT+ in simulating pulse recharge (reducing storm event error by 18.7%). Meanwhile, model simplification guided by parameter sensitivity (retaining four core parameters, including ALPHA_BF) reduces computational time by 57% while maintaining NSE > 0.91, demonstrating that physics-driven parameter selection can balance accuracy and efficiency. However, structural limitations are evident in three aspects:

(1) Vadose zone stratification simplification. The current model treats the 0–5 m vadose zone as a homogeneous layer, ignoring the water-blocking effects of clay-silt interlayers (in the northwest), leading to a positive bias in the simulated dry season depth at Changyuan-17 well by up to 0.38 m (Table 3);

(2) Insufficient quantification of human activities. Groundwater extraction for irrigation (annual average of 2.7×10^8 m^3) is represented only by empirical coefficients, lacking coupling with spatial heterogeneity of well distribution and extraction intensity;

(3) Absence of fracture flow mechanism. The preferential flow paths of bedrock fractures (Fengqiu-5 well area) are not explicitly depicted, resulting in a 3–5 day response delay during prolonged drought periods.

4.4 Implications for water resource management

The PD-SDO framework and its findings provide practical, science-based approaches to addressing water resource challenges in national strategic agricultural zones such as the study area. By linking model outputs to the core issues identified in the regional water resource assessment report of the "Zhongyuan Nonggu" project, the following management implications are derived:

(1) Implement targeted aquifer recharge. Through combined analysis of ALPHA_BF and GW_DELAY, areas with groundwater lag times of less than 120 days can be identified as optimal zones for Managed Aquifer Recharge (MAR). Implementing MAR strategies such as modified irrigation return flows and dedicated infiltration basins during the rainy season can improve recharge efficiency by more than 30%. The project report indicates that groundwater extraction in regions such as Yanjin County currently exceeds

the permitted quota, making this strategy critical for reversing ongoing groundwater exploitation. This framework provides a tool for spatially identifying these high-potential recharge zones and prioritizing their implementation.

(2) Adopt strategic land-use planning. Quantitative scenario analysis shows that 10% urban expansion reduces groundwater recharge by 18.7%, providing strong support for controlling construction land conversion. Conversely, increased forest cover enhances vadose zone water storage highlighting the co-benefits of ecological conservation for water security. Therefore, maintaining a net surplus of green infrastructure (woodland/grassland) relative to impervious surfaces is both an ecological goal and a groundwater resource management strategy. Spatial planning must fully account for these divergent hydrological impacts to prevent the loss of key recharge areas due to urbanization.

(3) Promote precision agricultural management. The model identifies CN2 as a highly sensitive parameter in the northeastern clay areas, which can be directly translated into management practices. Following model recommendations, promoting conservation tillage measures in these specific areas can increase infiltration rates by approximately 22%. Such measures reduce surface runoff and enhance precipitation infiltration, thereby lowering irrigation water demand and easing pressure on overexploited aquifers. This is a cost-effective, in-situ measure for improving water use efficiency at the field scale, complementing large-scale water resource allocation strategies.

(4) Reframe water security assessment under climate variability. This framework has a stronger ability to simulate pulse recharge generated by extreme rainfall (>50 mm/d), which is essential for assessing the reliability of water resource security. The project report shows that the region relies heavily on external water sources. Understanding the potential recharge value of increasingly variable and intense rainfall is critical for long-term water security planning. This model provides methodological support for evaluating the resilience of groundwater resources under non-stationary hydroclimatic conditions.

5 Conclusions

(1) The proposed Physics-Dominated Signal Decomposition Optimization (PD-SDO) framework, which integrates SWAT+ with ESMD, significantly enhances the accuracy and computational efficiency of groundwater simulations in intensively managed mixed land-use regions. By optimizing precipitation inputs to better capture extreme rainfall events, it achieves superior performance (NSE = 0.94) and greater physical interpretability compared to conventional models.

(2) Parameter sensitivity analysis identifies ALPHA_BF as the dominant parameter governing recharge dynamics, revealing the key role of dual-mode drainage in the loess vadose zone. A sensitivity-guided reduction of calibration parameters maintains high accuracy while markedly improving model efficiency.

(3) Land use scenario simulations quantify the contrasting hydrological impacts of afforestation (which enhances vadose zone storage) and urban expansion (which reduces recharge). The effects are spatially heterogeneous, underscoring the importance of aligning vegetation types with subsurface conditions for effective water resource management.

(4) This study provides practical guidance for managing groundwater in strategic agricultural zones, including targeted aquifer recharge, forest cover conservation, and the promotion of conservation tillage. Future work will focus on incorporating more detailed representations of human activities and subsurface heterogeneity to further enhance the framework's physical fidelity and utility.

Acknowledgement

This work was supported by the Key Scientific Research Project of Colleges and Universities in Henan Province (CN) [grant numbers 17A570004], the Henan Provincial Universities Scientific and Technological Innovation Team Supporting Programme Grant [24IRTSTHN012], the National Natural Science Foundation of China [51779093], and the North China University of Water Resources and Hydropower (NCUWH) Graduate Student Innovation Ability Enhancement Project [NCWUYC-202416011].

References

Abbas SA, Bailey RT, White JT, et al. 2024. A framework for parameter estimation, sensitivity analysis, and uncertainty analysis for holistic hydrologic modeling using SWAT+. Hydrology and Earth System Sciences, 28(1): 21−48. DOI：10.5194/hess-28-21-2024.

Abbas SA, White JT, Almahawis MK, et al. 2025. Dual-phase calibration for surface–subsurface hydrologic models with diverse hydrologic conditions. Journal of Hydrologic Engineering, 30(4): 04025019. DOI：10.1061/JHYEFF.HEENG-6479.

Bawa A, Mendoza K, Srinivasan R, et al. 2025. Enhancing hydrological modeling of ungauged watersheds through machine learning and physical similarity-based regionalization of calibration parameters. Environmental Modelling & Software, 186: 106335. DOI：10.1016/j.envsoft.2025.106335.

Chen S, Fu YH, Wu Z, et al. 2023. Informing the SWAT model with remote sensing detected vegetation phenology for improved modeling of ecohydrological processes. Journal of Hydrology, 616: 128817. DOI：10.1016/j.jhydrol.2022.128817.

Costa RCA, Santos RMB, Fernandes LFS, et al. 2023. Hydrologic response to land use and land cover change scenarios: An example from the Paraopeba River Basin based on the SWAT model. Water, 15(8): 1451. DOI：10.3390/w15081451.

Dai J, Pan L, Deng Y, et al. 2025. Modified SWAT model for agricultural watershed in Karst Area of Southwest China. Agriculture, 15(2): 192. DOI：10.3390/agriculture15020192.

Gu X, Long A, He X, et al. 2024. Response of runoff to climate change in the Manas River Basin flow-producing area, Northwest China. Applied Water Science, 14(3): 43. DOI：10.1007/s13201-023-02099-7.

Huang NE, Shen Z, Long SR, et al. 1998. The empirical mode decomposition and the Hilbert spectrum for nonlinear and non-stationary time series analysis. Proceedings of the Royal Society of London. Series A: Mathematical, Physical and Engineering Sciences, 454(1971): 903–995. DOI：10.1098/rspa.1998.0193.

Jahanshahi A, Asadi H, Gupta H. 2025. A data fusion approach to enhancing runoff simulation in a semi-arid river basin. Environmental Modelling & Software, 190: 106468. DOI：10.1016/j.envsoft.2025.106468.

Jeong H, Lee B, Kim D, et al. 2024. Improving estimation capacity of a hybrid model of LSTM and SWAT by reducing parameter uncertainty. Journal of Hydrology, 633: 130942. DOI：10.1016/j.jhydrol.2024.130942.

Luo Y, Chen J, Gao S, et al. 2017. Stability analysis of super-large-section tunnel in loess ground considering water infiltration caused by irrigation. Environmental Earth Sciences, 76(22): 763. DOI：10.1007/s12665-017-7106-7.

Ma J, Li Z, Ma B, et al. 2020. Determination of groundwater recharge mechanisms using stable isotopes in small watersheds of the Loess Plateau, China. Hydrogeology Journal, 29(2): 765–781. DOI：10.1007/s10040-020-02253-4.

Mosbahi M, Kassouk Z, Benabdallah S, et al. 2023. Modeling hydrological responses to land use change in Sejnane Watershed, Northern Tunisia. Water, 15(9): 1737. DOI：10.3390/w15091737.

Nguyen TV, Dietrich J, Dang TD, et al. 2022. An interactive graphical interface tool for parameter calibration, sensitivity analysis, uncertainty analysis, and visualization for the Soil and Water Assessment Tool. Environmental Modelling & Software, 156: 105497. DOI：10.1016/j.envsoft.2022.105497.

Re V, De Filippis G, Viaroli S, et al. 2020. Groundwater (Freeze and Cherry, 1979), ora disponibile anche in italiano. Acque Sotterranee - Italian Journal of Groundwater, 9(1): 89–90. DOI：10.7343/as-2020-453.

Rivera-Fernandez AS, Cotrina-Sanchez A, Salas López R, et al. 2025. Spatiotemporal land cover change and future hydrological impacts under climate scenarios in the Amazonian Andes: A case study of the Utcubamba River Basin. Land, 14(6): 1234. DOI：10.3390/land14061234.

Rong Y, Zeng S, Qin C, et al. 2024. Holistic parameter sensitivity: A new perspective to address the risk brought by multi-source deep uncertainty on watershed management. Journal of Environmental Management, 372: 122983. DOI：10.1016/j.jenvman.2024.122983.

Sang S, Li L. 2024. A stock prediction method based on heterogeneous bidirectional LSTM. Applied Sciences, 14(20): 9158. DOI：10.3390/app14209158.

Shishegar S, Ghorbani R, Saad Saoud L, et al. 2021. Rainfall–runoff modelling using octonion-valued neural networks. Hydrological Sciences Journal, 66(13): 1857−1865. DOI：10.1080/02626667.2021.1962885.

Shukla S, Meshesha TW, Sen IS, et al. 2023. Assessing impacts of Land Use and Land Cover (LULC) change on stream flow and runoff in Rur Basin, Germany. Sustainability, 15(12): 9811. DOI：10.3390/su15129811.

Talebizadeh M, Moriasi DN, Steiner JL, et al. 2024. Spatio-temporal sensitivity analysis for flow and sediment load modeling using SWAT in a heterogeneous agricultural watershed. Water Resources Management, 39(5): 2281−2298. DOI：10.1007/s11269-024-04066-6.

Valencia S, Villegas JC, Hoyos N, et al. 2024. Streamflow response to land use/land cover change in the tropical Andes using multiple SWAT model variants. Journal of Hydrology: Regional Studies, 54: 101888. DOI：10.1016/j.ejrh.2024.101888.

Wang JL, Li ZJ. 2013. Extreme-point symmetric mode decomposition method for data analysis. Advances in Adaptive Data Analysis, 5(3): 1350015. DOI：10.1142/S1793536913500155.

Wang K, Tan W, Si Y, et al. 2024. A solute transport in deformable dual-porosity media using mixture-coupling theory. Environmental Geotechnics, 11(3): 165−179. DOI：10.1680/jenge.22.00029.

Wu S, Dong Z, Guzmán SM, et al. 2024. Two-step hybrid model for monthly runoff prediction utilizing integrated machine learning algorithms and dual signal decompositions. Ecological Informatics, 84: 102914. DOI：10.1016/j.ecoinf.2024.102914.

Yilmaz AG, Muttil N, Adhikary SK. 2018. Improving streamflow forecast using optimal rain gauge network-based input to artificial neural network models. Hydrology Research, 49(5): 1559−1577. DOI：10.2166/nh.2017.108.

Yu H, Wen X, Feng Q, et al. 2017. Comparative study of hybrid-wavelet artificial intelligence models for monthly groundwater depth forecasting inextreme arid regions, Northwest China. Water Resources Management, 32(1): 301−323. DOI：10.1007/s11269-017-1811-6.

Zhang Q, Wu J, Liu W, et al. 2025. SWAT+ model enhanced with dynamic phenology remote sensing and high-precision precipitation data for water resource vulnerability assessment in semi-arid regions. Water Resources Management, 39(10): 4947−4969. DOI：10.1007/s11269-025-04182-x.